The Astrophysical Journal, 656:248–254, 2007 February 10

ON THE DISTANCE AND STRUCTURE OF W80

J. C. Cersosimo, R. J. Muller, S. Figueroa Vélez, N. Santiago Figueroa, and P. Baez
Department of Physics and Electronics, University of Puerto Rico at Humacao, Humacao, PR

and

J. C. Testori
Instituto Argentino de Radioastronomía, Buenos Aires, Argentina
Received 2005 October 10; accepted 2006 October 23

ABSTRACT

The continuum radiation of the Galactic region located at $l = 85^\circ$, $b = -0.5^\circ$ is well defined by its 11 cm emission. The region, extended 3° in diameter, is cataloged as W80, and its optical images show the North America and Pelican Nebulae complexes. In this paper we present new distance measurements and physical parameters obtained from radio recombination line observations at a frequency near 1.4 GHz. Four structures are identified in the region under study: a near structure is located at a distance of about 0.7 kpc, another structure lies on the east side of W80 at a distance of 1.7 kpc, there is a concentration of ionized gas on the west side at a distance of 2.7 kpc, and a fourth structure is found further away at 3.3 kpc, which does not seem to belong to the W80 complex. The results are presented using the (X, Y, Z)-coordinates of the Galactic plane. The model used assumes a constant electron temperature $T_e = 6800$ K and also assumes homogeneity. Our results seem to indicate that the ionized hydrogen of W80 spreads along the line of sight instead of clumping at one distance. We obtain values of the electron density and the ionization parameter between $n_e = 5$ and 16 cm^{-3} and $U = 51$ and 110 cm^{-2} pc, respectively.

Subject headings: Galaxy: disk — H II regions — ISM: individual (W80)

1. INTRODUCTION

An extended region of about 3° in diameter can be found at Galactic coordinates $l = 85^\circ$, $b = -0.5^\circ$; it is cataloged as W80 (Westerhout 1958). The region is well defined by the continuum emission at centimeter wavelength (Fürst et al. 1990), and is located in the line of sight of the Cyg OB6 and OB7 associations, which are part of the structure known as the Cygnus superbubble (Uyaniker et al. 2001). The region lies in the northeast part of the Cygnus X region. The optical counterpart includes the North America and the Pelican Nebulae (NPN), separated by a dust lane, L935 (Lynds 1962), which crosses the region in the north-south direction.

The W80 region was studied at decimeter wavelength by Wendker (1968). His conclusions suggest that the H II region consists of one extended component of uniform density distribution in which several local electron density enhancements are embedded. Other continuum studies in the region were carried out by Wendker et al. (1983), who estimate a distance of 500 pc for the NPN. Two supernova remnants (SNRs) were discovered by Kothes et al. (2001) superimposed on W80, G85.4+0.7 and G85.9−0.6. Polarization studies were made by Uyaniker et al. (2003); he suggests that the material of W80 depolarizes all extended nonthermal emission generated behind it, in agreement with the model set forth by Wendker et al. (1983).

The most difficult problem in the analysis of a continuum source is the discrimination between the emission of the thermal and nonthermal components. The determination of distances is also a difficult problem when we deal with continuum sources. Photometric distances of the H II region can be obtained by photometric data of the embedded hot star, but high optical extinction is a limitation. On the other hand, the determination of distances of H II regions by observation of radio recombination lines (RRLs) has been successful. Data of the high transition-level hydrogen emission has been obtained by searching the RRL emission using a small beam (Lockman 1989; Lockman et al. 1996). These observations are sensitive to gas of relatively high electron density ($n_e > 50$) when a combination of small antenna beam and high frequency (>5 GHz) is used.

We analyzed RRL observations over the W80 region at 1.4 GHz. These observations were obtained using a relatively large beam. One of the observations was obtained in the Galactic plane survey of Heiles et al. (1996) with a beam of $36'$. Data were also obtained as part of the survey at H166α by Azcárate et al. (1997) using a beam of $20'$ and from the observations of Barcia et al. (1985) with a beam of $20'$. All data were obtained using a single dish antenna and almost at the same frequency (1.4 GHz).

These observations are sensitive to the Extended Low Density Warm Ionized Medium (ELDWIM; Petuchowski & Bennett 1993; Heiles 1994). This component covers a significant portion of the interstellar medium and is found from the Galactic center to a distance close to 13 kpc (Mezger 1978). The radial extension of this component, as mapped by optical Hα observations, is poorly constrained for distances from 1 to 2 kpc from the Sun, due to interstellar absorption (e.g., Reynolds 1983). Unrestricted by interstellar absorption, hydrogen RRLs such as H166α are sensitive to gas with relatively low electron density ($0.3 < n_e < 50$) spread across large volumes. These ionized regions are characteristic of the ELDWIM. However, these observations can be used to trace the radial distribution of the ELDWIM, as was done in the northern Galactic plane (Hart and Pedlar 1976; Lockman 1976; Heiles et al. 1996) and in the southern Galactic plane (Cersosimo et al. 1989).

We attempt to identify the thermal gas of the continuum structure of W80, which should potentially be the source of RRLs. We analyzed the line-emission data in order to derive the distance of the emitting gas by applying a flat rotation-curve model. The kinematic distance allows us to obtain the physical parameters of the region.

2. THE H166α LINE EMISSION FROM W80

In the left panel of Figure 1, we show the map of radio continuum observed by Fürst et al. (1990). The 11 cm emission does

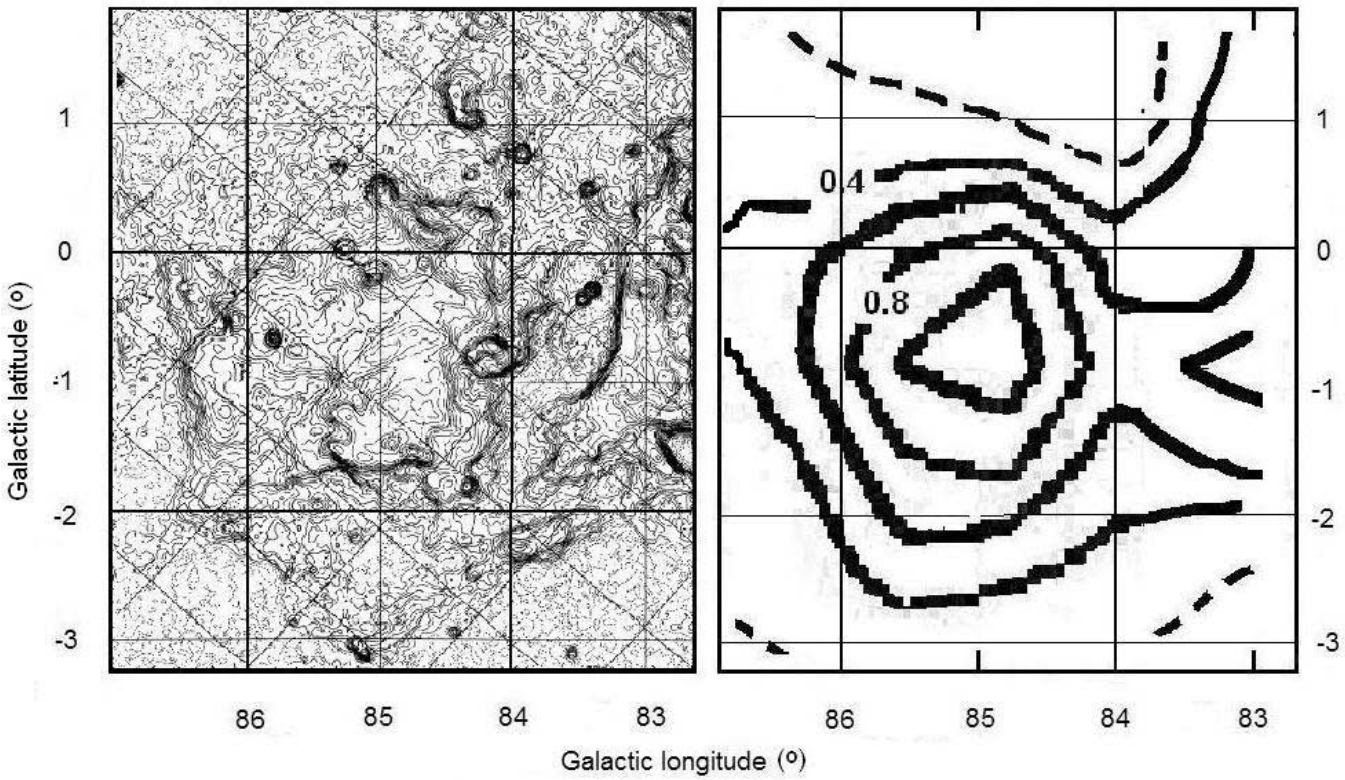

FIG. 1.—*Left*: Continuum image at 11 cm (Fürst et al. 1990). *Right*: Integrated emission of the H166α radio recombination line between -90 and +90 km s^{-1} (Azcárate et al. 1997).

not present a unique simple maximum; the emission is composed of various structures with the appearance of long filaments. The right panel of Figure 1 shows the map of the integrated RRLs between velocities -90 and +90 km s^{-1} observed over twelve positions by Azcárate et al. (1997). These figures allow us to see the spatial correlation between the continuum emission and the distribution of the line emission. The contour map of the integrated RRLs over the region, which is extended from 83.5° to 87° in longitude and from $-3°$ to +0.5° in latitude, has a peak emission located around the position $l = 85°$, $b = -0.5°$; the emission line vanishes at the positions where the 11 cm continuum also does.

Additional observations of the H166α line emission from W80 were made by Heiles et al. (1996), who observed the line at six positions. Another observation over three positions was carried out by Barcia et al. (1985). The observations and the parameters obtained from the samples are described in Table 1. Column (1) shows the Galactic position's name; column (2) shows the peak temperature of the line. Columns (3) and (4) show the width and the peak's velocity of the profiles, respectively. Column (5) shows the kinematic distance, column (6) shows the *Z*-height with respect to the Galactic plane, and column (7) lists the references.

3. DETERMINATION OF DISTANCE

One of the relevant parameters needed to understand the structure of the W80 complex is distance. This is also the most difficult parameter to estimate with any accuracy. We obtained the distance by the kinematic method using the peak's velocities of the H166α line observations. Figure 2 shows the variation of $V_{\rm LSR}$ with distance as a function of the Galactic longitude. The distances are obtained using a "flat" rotation curve with $R_0 =$ 8.0 kpc (Reid 1993) and $V_0 = 220$ km s^{-1}. The curves show the presence of distance ambiguity for positive velocities but show no distance ambiguities for negative velocities.

The velocities of the profiles were obtained from a Gaussian fit to the lines (Heiles et al. 1996; Azcárate et al. 1997; Barcia et al. 1985). Column (4) of Table 1 shows positive velocities for three positions. The velocities of two of them (G84.0$-$1.5 and G85.0$-$1.5) should correspond to the maximum of the rotation curves, so we assume that the gas is located at the tangential point of the Galactic rotation. The velocity of the emission at G84.5$-$1.25 is +0.9 km s^{-1}. According to the flat-rotation galactic model, this implies an ambiguity for distance determination. The near distance corresponds to 0.5 kpc, and the far distance to 1.4 kpc. We adopt the near distance arbitrarily because this value is consistent with the results of Straižys et al. (1989). For the positions where we have more than one observation, the parameters of the profiles were averaged.

We obtained the *Z*-height of the emission (defined as usual: $Z = D \sin b$) and the projection onto the Galactic plane ($X = D \cos l$ and $Y = D \sin l$) once the distance to the Sun D was computed for all positions. In this reference system, the Sun is at the origin, the *X*-axis is pointing to the Galactic center, and the *Y*-axis is pointing toward longitude $l = 90°$. Figure 3 summarizes the results; it shows the distribution of the emission at the three Galactic coordinates. Each point corresponds to the emission of each profile described in Table 1. The upper panel of Figure 3 presents the *Z*-height of the emission versus the *Y*-projection. This figure shows the emission localized between 0.5 and 3.2 kpc and the distribution on the *Z* height between -40 and +40 pc.

The lower panel of Figure 3 shows the emission on the (X, Y)-plot. It can be inferred from Figure 3 that the ionized gas is clumped at different distances. We obtained the average velocity from the peak velocity of the profiles and computed the most

TABLE 1
PARAMETERS OF RRL FROM SINGLE-DISH OBSERVATIONS NEAR 1.4 GHz

Source Name (1)	T_L (mK) (2)	Δv (km s^{-1}) (3)	v (km s^{-1}) (4)	D (kpc) (5)	Z (kpc) (6)	References (7)
G84.0−1.5[a]	95	24.23 ± 3	+3.18 ± 3	0.9 ± 0.5	−19 ± 10	1
G84.0−0.6	49	18.7 ± 3	−3.9 ± 3	2.4 ± 0.5	−25 ± 6	2
G84.0−0.5	66	20.04 ± 2	−5.46 ± 3	2.6 ± 0.4	−22 ± 6	1
G84.0+0.0[b]	36.5	26.4 ± 4	−5.6 ± 3	2.7 ± 0.4	0 ± 4	1, 3
G84.0+0.5	18	24.07 ± 2	−9.42 ± 3	3.3 ± 0.3	+26 ± 4	1
G84.0+0.8	28.8	18.2 ± 2	−8.7 ± 2	3.2 ± 0.3	+39 ± 4	2
G84.5−1.25[c]	82	20.4 ± 2	+0.9 ± 3	0.5 ± 0.4	−8 ± 7	2
G84.6−0.6	129	19.6 ± 2	−2.8 ± 3	2.2 ± 0.5	−21 ± 5	2
G85.0−1.5[a]	41	22.88 ± 2	+2.65 ± 3	0.6 ± 0.5	−16 ± 8	1
G85.0−0.5	117	21.75 ± 2	−0.74 ± 3	1.7 ± 0.5	−13 ± 4	1
G85.0+0.0[b]	88.5	20.7 ± 2	−0.62 ± 3	1.6 ± 0.5	0 ± 5	1, 3
G85.0+0.5	27	29.54 ± 4	−2.07 ± 3	1.9 ± 0.5	+16 ± 11	1
G85.8−0.6	88	16.9 ± 2	−3.9 ± 2	2.1 ± 0.4	−22 ± 5	2
G86.0−1.5	42	24.98 ± 4	−0.97 ± 3	1.5 ± 0.5	−35 ± 5	1
G86.0−0.5	62	25.15 ± 4	−0.61 ± 3	1.3 ± 0.5	−10 ± 4	1
G86.0+0.0[b]	37	24.4 ± 2	−2.0 ± 3	1.7 ± 0.5	0 ± 4	1,3
G86.0+0.5	24	19.46 ± 2	−1.72 ± 3	1.6 ± 0.5	+13 ± 5	1
G86.16−1.25	30	30.5 ± 2	−2.4 ± 3	1.8 ± 0.5	−39 ± 10	2
G87.0+0.0[d]	21	80.87 ± 5	+6.93 ± 6	...	...	1
G87.0−0.5[d]	18	61.79 ± 5	+12.42 ± 6	...	...	1

[a] Distance obtained from the tangent point.
[b] Average of two observations.
[c] Near distance.
[d] Very wide line, no kinematic data may be obtained.
REFERENCES.—(1) Azcárate et al. 1997; (2) Heiles et al. 1996; (3) Barcia et al. 1985.

probable distance for each of these clumps. One of them is located at 0.7 kpc and at a Z-height of −10 pc. An extended structure is located around 1.7 kpc and is vertically extended from $Z = -40$ to $Z = +20$ pc. Another object is located at 2.7 kpc, extended from $Z = -25$ to $Z = 0$ pc. A more distant emission is found at 3.3 kpc and $Z = +30$ pc.

Figure 4 shows the structures projected on the optical image of the Palomar Observatory Sky Survey (POSS). It shows the NPN, which are known as S117. The positions where the RRLs have been observed are shown; squares, dots, and plus signs indicate the positions of each line emission as detected by Heiles et al. (1996), Azcárate et al. (1997), and Barcia et al. (1985), respectively.

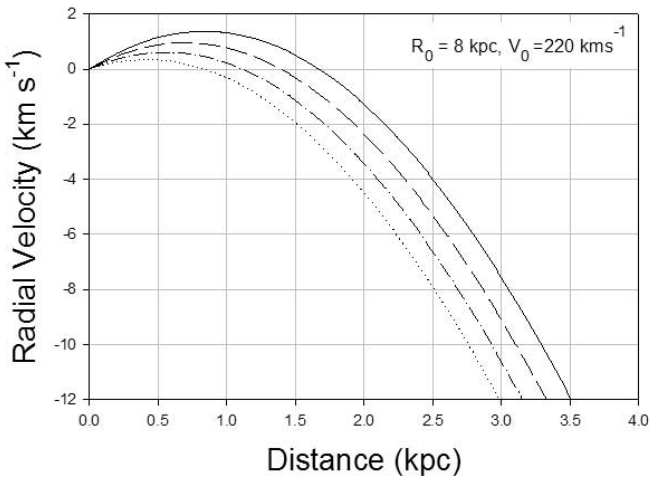

FIG. 2.—Distance vs. radial velocity as a function of Galactic longitude. Solid, dashed, dash-dotted, and dotted curves correspond to 84°, 85°, 86°, and 87°, respectively. Calculations were made assuming $R_0 = 8.0$ kpc and $V_0 = 220$ km s^{-1} (Reid 1993).

We indicate the location of the different RRL emissions by overlapping the samples with the optical image in Figure 4. They are identified by two ovals and a circle. The horizontal oval indicates the source found at a distance of 0.7 ± 0.5 kpc. It is projected onto the southwest of W80, just at the end of the optical dust filament. The RRL emission emerging from this area is probably associated with the optical feature, the "Yucatan peninsula." The vertical oval on the west of the NPN shows the emission located between 2.5 and 2.9 kpc, shown in the bottom panel of Figure 3. Its average velocity, obtained from the profiles, is $v = -5.12 \pm 0.73$ km s^{-1}, which corresponds to a distance of 2.7 ± 0.3 kpc.

The circle in the northwest shows the location of the line emission emerging from the northwest of the NPN. The average peak velocity is −9.10 ± 0.34 km s^{-1}, and the flat rotation-curve model of Figure 2 suggests that the gas is located at a distance of 3.3 ± 0.3 kpc. The emission is found above the Galactic plane at $Z = +40$ pc and seems to be emerging from the continuum spots located at $l = 84.0°, b = 0.5°$ and $l = 84.0°, b = 0.8°$ (Fürst et al. 1990), which do not belong to W80.

There is an additional emission source emanating from the remaining region, projected over the east side of the NPN. It has an average velocity of −1.70 ± 1.20 km s^{-1}; this velocity corresponds to a distance of 1.7 ± 0.4 kpc. The vertical extension of this emission is around 60 pc, from $Z = -40$ to +20 pc.

4. PHYSICS OF THE LINE EMISSION

The line intensity T_L at the peak of the line is a function of the electron temperature T_e, the electron density n_e, and the emission measure E, which is defined by

$$E = \int n_e^2 \, ds, \tag{1}$$

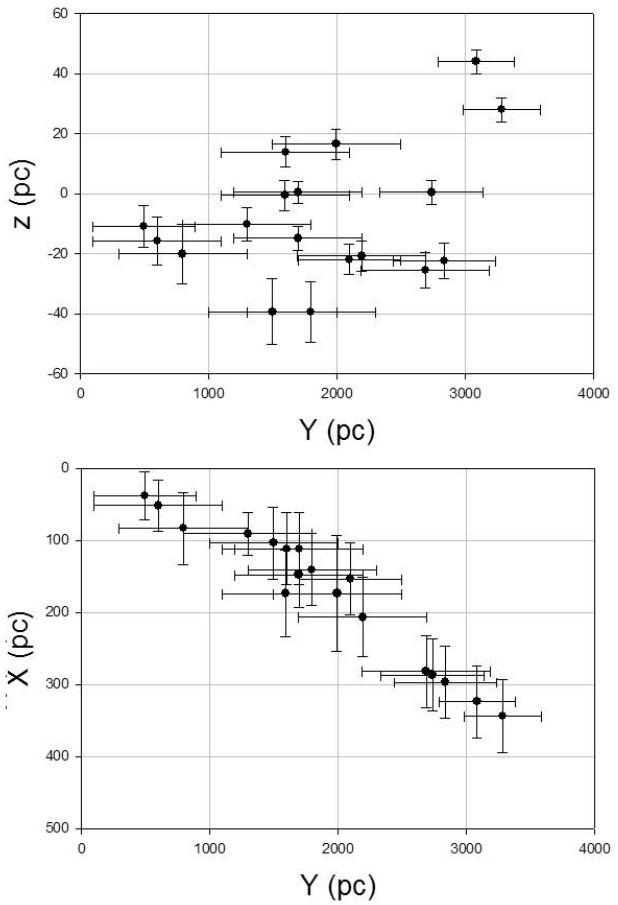

FIG. 3.—Plots of the emission at the (X, Y, Z)-coordinates of the Milky Way; each point represents profiles from the RRL emission. The X-coordinate is pointing toward the Galactic center and the Y-coordinate is pointing toward $l = 90°$. The Sun is at the origin of the coordinate system. The projection onto the (Z, Y)-plane shows the vertical distribution as a function of the Y-coordinates (*upper panel*). The distribution on the Galactic plane is shown by the (X, Y)-projection (*lower panel*).

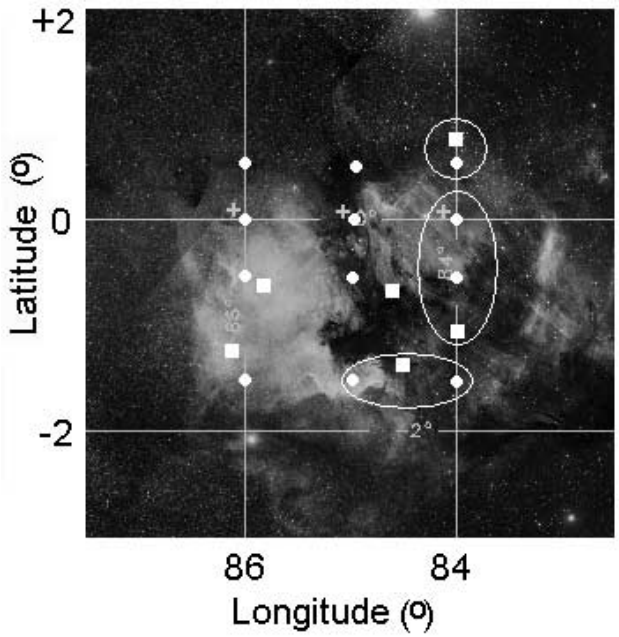

FIG. 4.—Optical image of the NPN from the Digitized Sky Survey. Dots show the targets of Azcárate et al. (1997), squares show the targets of Heiles et al. (1996), and plus signs show the targets of Barcia et al. (1985). The horizontal oval shows the near region located at about 700 pc, over the "Yucatan peninsula," which is associated with the dark clouds L935. The vertical oval shows the region where the line velocities suggest a distance larger than 2.7 kpc. The circle shows the profiles with high negative velocities, from which a distance of 3.3 kpc is obtained. In the region over the "USA shape" and the "head of the Pelican" (northeast), the profiles suggest an average distance of 1.7 kpc.

where s is the path length along the line of sight. If we assume homogeneity and also assume that the line arises under conditions of local thermodynamic equilibrium (LTE), the optical depth is given by (Shaver 1976)

$$\tau_L^* \simeq 4.61 \times 10^{-4} \frac{E}{\Delta v T_e^{5/2}} n^3 \left(\frac{f_{m,n}}{n}\right) \times \exp\left(\frac{1.58 \times 10^{-5}}{n^2 T_e}\right)(1 + 1.48\gamma)^{-1}, \quad (2)$$

where the emission measure E is in cm^{-6} pc, n is the quantum number, Δv is the full Doppler profile in km s^{-1}, $f_{m,n}$ is the oscillator strength from Menzel (1969), and T_e is the electron temperature in K. The factor γ is the ratio of the profile width due to Stark broadening to that due to pure Doppler broadening, which depends strongly on the electron densities and the quantum number. We obtain $\gamma \leq 8 \times 10^{-3}$ for rarified gas (Brocklehurst & Seaton 1972).

Given the fact that the nebula is optically very thin, we can write the temperature as

$$T_L/\eta_B = \tau_L^* T_e, \quad (3)$$

where the asterisk indicates that the line is formed under LTE conditions. The factor η_B is the beam efficiency; it is equal to 0.71 for the 43 m Robert C. Byrd Green Bank Telescope and 0.8 for the 26 m antenna at Hart Creek (C. Heiles 2006, private communication). However, for $n = 166$, one can derive an average emission measure over the radio beam,

$$E \simeq 2.48 \times 10^{-3} \frac{T_L \Delta v}{\eta_B} T_e^{+1.5}. \quad (4)$$

We computed the emission measure for each profile and then obtained the averaged results for each object described in Figure 4.

Departure from LTE has been discussed by Shaver (1980); in his conclusions he suggests that there is no evidence of significant deviations from LTE effects. If we assume that the line is arising under LTE conditions, by substituting equation (2) into equation (3), the emission measure as a function of the line power $T_L \Delta v$ is obtained.

Stars of high surface temperature are sources of strong ultraviolet radiation; in the vicinity of these stars, hydrogen is ionized by photons shortward of 912 Å. Since the lifetime of the H II region is relatively short (Osterbrock 1989), we can assume that the hot stars ionizing the hydrogen gas are on the zero-age main sequence (ZAMS) and have their spectral types according to some initial mass function (IMF). Then we may compute the total mass of ZAMS stars associated with a certain Lyman photon flux, $N_{\rm Lyc}$, which depends mainly on the surface temperatures of the stars, obtained from their spectral types.

The effective radius of the ionized region will be such that the total ionization rate caused by the stars should just be equal to the total recombination rate of the surrounding H II region. We use

TABLE 2
PHYSICAL PARAMETERS OF THE W80 REGION

Object (1)	Average Velocity (km s^{-1}) (2)	D (kpc) (3)	S (pc) (4)	$\langle E \rangle$ (cm^{-6} pc) (5)	$\langle n_e^2 \rangle^{1/2}$ (cm^{-3}) (6)	U (cm^{-2} pc) (7)	$N_{\rm Lyc}$ (10^{48} s^{-1}) (8)	O8 Stars (9)
Horizontal oval	$+2.24 \pm 0.9$	0.7 ± 0.5	12	3100 ± 1500	16 ± 6	51	6	<2
Northeast region	-1.70 ± 1.20	1.7 ± 0.4	60	2600 ± 600	7 ± 3	110	63	16
Vertical oval	-5.12 ± 0.73	2.7 ± 0.3	47	1900 ± 200	6 ± 2	82	26	6
Circle	-9.10 ± 0.34	3.3 ± 0.3	44	900 ± 100	5 ± 1	64	12	3

the following definition of the excitation parameter (U), which is a function of the spectral type:

$$U = s_0 \langle n_e^2 \rangle^{1/3}, \quad (5)$$

where s_0 is the effective radius of the H II region. Strömgren (1939) has further shown that it depends only on the flux of Lyman continuum photons from the exciting star. However, in order to obtain an estimate of U, we must assume that (1) the RRL emission arises from thermal ionized gas, and spontaneous emission is the main process; (2) the gas is ionized by the flux of Lyman continuum photons from the exciting stars; and (3) the electron temperature at the galactocentric distance of W80 is $T_e = 6800 \pm 300$ K. This value is adopted from the slope of the electron temperature versus the Galactic radius, derived by Paladini et al. (2004).

The path length of the emission was obtained from the angular size and the distance for each region described in § 3. The electron density was obtained from the equation

$$\sqrt{\langle n_e^2 \rangle} = \sqrt{E/s}, \quad (6)$$

which is related to density inhomogeneities along the line of sight (however, it should be the case that $\langle n_e^2 \rangle < n_e^2$). Finally, one obtains the excitation parameter

$$U = \frac{s}{2} \langle n_e^2 \rangle^{1/3}, \quad (7)$$

where $s = 2s_0$. Since $N_{\rm Lyc}$ is proportional to U^3, the photon Lyman flux ionizing the hydrogen gas is obtained from (Spitzer 1978)

$$N_{\rm Lyc} = 2.086 \times 10^{46} U^3 T_e^{-0.698}, \quad (8)$$

where the recombination coefficient $\alpha^{(2)}{}_0$ has been approximated by $1.69 \times 10^{-10} T_e^{-0.698}$ from the value tabulated by Spitzer (1978).

In summary, we computed the average velocity and then the distance for each region described in § 3. The emission measure for each object was obtained from the power of the line and by using equation (4), assuming an electron temperature of $T_e = 6800$ K. The electron density and the excitation parameter were computed from equations (6) and (7) using a path length obtained from angular size and distance. Finally, we obtained the photon flux needed to ionize each region using equation (8).

In Table 2 we show the results; column (1) describes the objects, column (2) shows the average velocity and its standard deviation. Columns (3) and (4) show the distance and the size of each region, respectively. Column (5) shows the average emission measure, column (6) shows the electron density, column (7) shows the excitation parameter, and column (8) shows the photon production rate of O stars associated with the ELDWIM, in units of 10^{48} s^{-1}. From these data we obtain the number of O8 (low-mass) stars needed to inject the ionizing energy (Osterbrock 1989). They are shown in column (9).

5. DISCUSSION

Early work has suggested that the value of the distance to the NPN falls in the range from 0.2 to 1 kpc (Neckel et al. 1980; Armandroff & Herbst 1981). Wendker et al. (1983) estimates a distance of 500 pc for the NPN from a model suggesting a group of eight early-type stars ionizing so-called cavities in the parent molecular cloud. From this model, Uyaniker et al. (2003) justified Faraday rotation, assuming a density varying from 6 to 40 cm^{-3} and a path length of 35 pc. However, optical measurements suggest a distance of 1 kpc (Georgelin & Georgelin 1970, 1976). Our data suggest a more complicated picture. We find a structure of ionized gas projected over different positions and located at different distances. The main controversy pertains to the W80 radio source that is projected onto the optical image of the NPN. Up to now it has been considered to be a single structure. Our kinematic data suggest that it is composed of three gaseous structures along the line of sight between 0.7 and 2.7 kpc. The lower panel of Figure 3 shows the localization of the gas in the (X, Y)-plot. The emission is located in a curved distribution on the Galactic plane in such a manner that the emission seems to occur at the same distance from the Galactic center. The line emission is located at the near side of the local spiral arm traced by atomic hydrogen (McCutcheon & Shuter 1970). Although the longitude range studied in this paper is only 3° in extension, our results are in agreement with the interpretation of Bochkarev & Sitnik (1985). They argue in favor of the spiral arm structure in the region.

The ionized gas studied here is located at the east side of the superbubble object, but the expanding behavior is not evident from Figure 3. The radio recombination lines (RRLs) suggest that W80 is composed of objects located at different distances that seem to be localized behind L935, an obscuring gas-dust system (Straižys et al. 1989).

The feature shown by the horizontal oval lies projected over the "Yucatan peninsula" optical feature at the south of the dark filament studied by Uyaniker et al. (2003). The distance reported here is in agreement with the findings of Straižys et al. (1989). The electron density obtained for this object is 16 ± 6 cm^{-3}, and the photon flux needed to ionize the region is about 6×10^{48} s^{-1}. We suggest that the H II region is associated with the dust lane (Straižys et al. 1989) at the south part of L935. Since Cygnus OB7 is a nearby star association, located at 0.7 kpc (Mel'Nik & Efremov 1995), the ionization sources could be some members of the Cygnus OB7 association embedded in the ionized gas.

The line emission projected on the "USA shape" and the "head of the Pelican" of the NPN (at the northeast of W80) is located at a distance of about 1.7 ± 0.4 kpc. According to Mel'Nik & Efremov (1995), the gas is being ionized by the Cygnus OB6

association (Uyaniker et al. 2003 states that the 1.6 kpc distance of this stellar association is doubtful).

The profiles of the horizontal oval and the northeast regions shown in Figure 4 have low negative velocities. Their errors are larger than their absolute values. This fact makes it difficult to calculate the distance. For example, the source G85.0−0.5 (see Table 1) has a velocity of -0.74 ± 3.0 km s^{-1}; based on this uncertainty the distance range would fall between 0 and 2.3 kpc. There are three positions with velocities between +1 and −1 km s^{-1}, and all of the members of this group show uncertainties larger than their absolute values. Furthermore, there are measurements at G85.8−0.6 and G86.0−0.5, which were observed about 13′ apart. This separation is significantly smaller than the beam, yielding quite different observed radial velocities of -3.9 ± 2.0 and -0.61 ± 3.0 km s^{-1}, respectively. We also found that the two positions with high positive velocities (G84.0−1.5 and G85.0−1.5), which are assumed to be at the tangent point, have observed velocities that are almost 2 km s^{-1} above the tangent-point velocity.

Let us assume that these two emitting regions (the horizontal oval and the northeast region in Fig. 4) correspond to a unique object. The average velocity of the profiles is $\langle v \rangle = -0.92$ km s^{-1}, with a standard deviation $\sigma = 2$ km s^{-1}. Based on this velocity uncertainty, the 1 σ distance range is between 0.5 and 2.2 kpc. These uncertainties would be caused by random motion within the region. The possibility that these groups are actually located at the same distance should in turn imply that the results would actually agree with earlier distance estimates.

The vertical oval in Figure 4 shows the line emission located on the northwest corner of W80, just over a high gradient of a continuum radiation feature (Fürst et al. 1990) around G84−0.8, recognized as a SNR (Matthews et al. 1977). The distance obtained from the RRL emission is 2.7 ± 0.3 kpc. This thermal source seems to be located far away from the structures discussed before. The physical parameters shown in Table 2 suggest the presence of typical extended low-density ionized gas with $N_{\rm Lyc} = 2.6 \times 10^{49}$ s^{-1}.

Molecular gas is also prevalent in the W80 region (Leung & Thaddeus 1992), and it is located at the east of the X-ray superbubble. Kothes et al. (2001), inspecting the *ROSAT* data, noticed very high absorption in the direction of the SNRs G85.4+0.7 and G85.9−0.6. Our results suggest the presence of low-density ionized gas with densities of 16, 7, and 6 cm^{-3} for each structure, respectively, and a total number of ionizing photons $N_{\rm Lyc} \sim 10^{50}$ s^{-1} for the W80 complex. We assumed homogeneity in both the density and the electron temperature. These models are crude, and of course they are not unique. The estimate of the excitation parameter is uncertain because the size of the nebula projected onto the sky does not match the distribution of the emission along the line of sight.

We would like to state the fact that the emission of the RRLs shows a vertical distribution and is also correlated with molecular cloud emission (Leung & Thaddeus 1992). Furthermore, young stars are present (Mel'Nik & Efremov 1995). This picture needs to be investigated further. The results of columns (7) and (8) of Table 2 suggest the amount of ionization energy needed to ionize the hydrogen gas. This energy is a fraction of the total amount. It represents a lower limit because the model does not take into account the photons heating the molecular clouds.

6. CONCLUSION

The ionized gas projected over the W80 radio source shows three concentrations located at different distances. The near region is located at 0.7 ± 0.5 kpc (Fig. 4, *horizontal oval*). The gas is seen at the southern part of the 11 cm continuum spot. Our results suggest that the ionized hydrogen and the dark region (Lynds 935) are associated. The kinematic distance suggests that the radio recombination line originates in ionized gas being excited by members of the Cygnus OB7 association.

The ionized gas on the northeast side of the region is located at 1.7 ± 1.2 kpc. This region is vertically extended from $Z = -50$ to +20 pc.

The emission of ionized gas on the west of W80 (Fig. 4, *vertical oval*) shows the thermal gas at a distance of 2.7 ± 0.3 kpc and vertically extended from the Galactic plane to $Z = -30$ pc.

The more distant emission (Fig. 4, *circle*) is located at 3.3 ± 0.3 kpc and at a Z-height of about 40 pc. This feature is correlated with a continuum spot at the north of W80, and the object is not part of the W80 complex. The electron density obtained is about 5 ± 1 cm^{-3}.

The spatial correlation between the 11 cm emission and the emission of the RRLs at 1.4 GHz suggests that both emissions arise from the same gas and also reveals the thermal nature of the region. The W80 region consists of low-density ionized gas spread at different distances in the range between 0.7 and 2.7 kpc. It further strengthens the hypothesis that the ionized gas of W80 is distributed along the line of sight instead of being clumped at one distance.

This research was supported by NASA Training Grant NNG05GG78H (PR Space Grant) and NASA Cooperative Agreement NCC5-595 (PR NASA EPSCoR). We are grateful to Carl Heiles for providing technical information about the instrumentation used in early surveys.

The Digitized Sky Survey was produced at the Space Telescope Science Institute under US government grant NAG W-2166. The images of these surveys are based on photographic data obtained using the Oschin Schmidt Telescope on Palomar Mountain and the UK Schmidt Telescope. The plates were processed into the present compressed digital form with the permission of these institutions.

REFERENCES

Armandroff, T. E., & Herbst, W. 1981, AJ, 86, 1923
Azcárate, I. N., Cersosimo, J. C., Wilkes, L. N., & Cordero, Y. A. 1997, Ap&SS, 253, 313
Barcia, A., Gómez-González, J., Lockman, F. J., & Planesas, P. 1985, A&A, 147, 237
Bochkarev, N. G., & Sitnik, T. G. 1985, Ap&SS, 108, 237
Brocklehurst, M., & Seaton, M. J. 1972, MNRAS, 157, 179
Cersosimo, J. C., Azcárate, I. N., Hart, L., & Colomb, F. R. 1989, A&A, 208, 239
Fürst, E., Reich, W., Reich, P., & Reif, K. 1990, A&AS, 85, 691
Georgelin, Y. M., & Georgelin, Y. P. 1976, A&A, 49, 57
Georgelin, Y. P., & Georgelin, Y. M. 1970, A&A, 6, 349
Hart, L., & Pedlar, A. 1976, MNRAS, 176, 547
Heiles, C. 1994, ApJ, 436, 720
Heiles, C., Reach, W. T., & Koo, B. 1996, ApJ, 466, 191
Kothes, R., Landecker, T. L., Foster, T., & Leahy, D. A. 2001, A&A, 376, 641
Leung, H. O., & Thaddeus, P. 1992, ApJS, 81, 267
Lockman, F. J. 1976, ApJ, 209, 429
———. 1989, ApJS, 71, 469
Lockman, F. J., Pisano, D. J., & Howard, G. J. 1996, ApJ, 472, 173
Lynds, B. T. 1962, ApJS, 7, 1
Matthews, H. E., Baars, J. W. M., Wendker, H. J., & Goss, W. M. 1977, A&A, 55, 1
McCutcheon, W. H., & Shuter, W. L. H. 1970, AJ, 75, 910
Mel'Nik, A. M., & Efremov, Y. N. 1995, Astron. Lett., 21, 10
Menzel, D. H. 1969, ApJS, 18, 221

Mezger, P. G. 1978, A&A, 70, 565
Neckel, T., Harris, A. W., & Eiroa, C. 1980, A&A, 92, L9
Osterbrock, D. E. 1989, Astrophysics of Gaseous Nebulae and Active Galactic Nuclei (Mill Valley: Univ. Science Books), 24
Paladini, R., Davies, R. D., & DeZotti, G. 2004, MNRAS, 347, 237
Petuchowski, S. J., & Bennett, C. L. 1993, ApJ, 405, 591
Reid, M. J. 1993, ARA&A, 31, 345
Reynolds, R. J. 1983, ApJ, 268, 698
Shaver, P. A. 1976, A&A, 49, 1
———. 1980, A&A, 91, 279
Spitzer, L., Jr. 1978, Physical Processes in the Interstellar Medium (New York: John Wiley & Sons), 105
Straižys, V., Goldberg, E. P., Meistas, E., & Vansevicius, V. 1989, A&A, 222, 82
Strömgren, B. 1939, ApJ, 89, 526
Uyaniker, B., Fürst, E., Reich, W., Aschenbach, B., & Wielebinski, R. 2001, A&A, 371, 675
Uyaniker, B., Landecker, T. L., Gray, A. D., & Kothes, R. 2003, ApJ, 585, 785
Wendker, H. J. 1968, Z. Astrophys., 68, 368
Wendker, H. J., Benz, D., & Baars, J. W. M. 1983, A&A, 124, 116
Westerhout, G. 1958, Bull. Astron. Inst. Netherlands, 14, 215